Earth's oldest evolved rocks are impact melts

Tim E. Johnson[1,2]*, Nicholas J. Gardiner[1], Katarina Miljković[1], Christopher J. Spencer[1], Christopher L. Kirkland[1], Phil A. Bland[1] and Hugh Smithies[3]

[1]School of Earth and Planetary Sciences, The Institute for Geoscience Research (TIGeR), Curtin University, Perth, Western Australia 6845, Australia.

[2]Center for Global Tectonics, State Key Laboratory of Geological Processes and Mineral Resources, China University of Geosciences, Wuhan, Hubei Province, 430074, China.

[3]Geoscience Directorate, Department of Mines, Industry Regulation and Safety, 100 Plain Street, East Perth, WA 6004, Australia.

*e-mail: tim.johnson@curtin.edu.au

Earth's oldest evolved (felsic) rocks, the 4.02 billion-year-old Idiwhaa gneisses of the Acasta Gneiss Complex, northwest Canada, have compositions that are distinct from the felsic rocks that typify Earth's ancient continental nuclei, implying they formed through a different process. Using phase equilibria and trace element modelling, we show that the Idiwhaa gneisses were produced by partial melting of iron-rich hydrated basaltic rocks (amphibolites) at very low pressures, equating to the uppermost ~3 km of a Hadean crust that was dominantly mafic in composition. The heat required for partial melting at such shallow levels is most easily explained through meteorite impacts. Hydrodynamic impact modelling shows that, not only is this scenario physically plausible, but the region of shallow partial melting appropriate to formation of the Idiwhaa gneisses would have been

widespread. Given the predicted high flux of meteorites in the late Hadean, impact melting may have been the predominant mechanism that generated Hadean felsic rocks.

The Hadean and earliest Archean eons (~4.5 to 3.9 billion years ago) witnessed a barrage of asteroid impacts that caused global-scale melting and recycling of Earth's surface[1-3]. Although ~3.7 billion-year-old rocks are known to have existed within most continental nuclei, and there are rare vestiges of still older Archean crust[4], there is almost no crustal material preserved from the Hadean, Earth's formative eon.

Much of our understanding of the Hadean Earth comes from studies of tiny grains (<<1 mm) of the mineral zircon, which have radiometric ages that extend back to ~4.4 Ga[5]. The trace element and isotopic composition of Hadean zircons provide compelling evidence for the existence of surface water[5-7]. Although some also interpret chemical and mineral inclusion data from Hadean zircon as evidence for significant volumes of evolved (felsic) continental crust[8-10], others posit that Earth's crust in the Hadean was dominantly of basaltic (mafic) composition[11-13].

The only known felsic rocks of Hadean age occur within the Acasta Gneiss Complex (AGC), part of the Slave Craton of northwest Canada[14,15]. Its oldest dated components, the 4.02 Ga Idiwhaa tonalite gneisses[11,16,17], are magnetite-rich felsic gneisses with chemical compositions clearly distinct from rocks of the tonalite–trondhjemite–granodiorite (TTG) suite that dominate exposed Archaean crust worldwide (Fig. 1)[18]. These compositional differences suggest a different petrogenesis[17]. The AGC also contains abundant amphibolite, hydrated mafic rocks from which the felsic rocks may have been derived through partial melting[11,19,20]. In particular, the Idiwhaa gneisses are spatially associated with Fe-rich amphibolites, which now contain garnet that formed during a subsequent episode of metamorphism at 3.65–3.60 Ga[19,21].

47 Although the age of the mafic components of the AGC is unknown, some are intruded by felsic
48 rocks and are considered to be Hadean in age[19,21].

49 Compared to TTGs (average SiO_2 = 69 wt%, Al_2O_3 ~15 wt%, average FeO_T = 2.7 wt%),
50 which include most of the younger (3.93–2.94 Ga) Acasta felsic gneisses, the Idiwhaa gneisses
51 range to lower silica contents (70–58 wt.%) and Mg# [most are <20; Mg# = atomic Mg/(Fe +
52 Mg)], marginally lower Al_2O_3 (~13 wt.%) and much higher FeO_T (8–15 wt.%)[17] (Fig. 1a,b;
53 Supplementary Table 1). The high FeO contents, low Mg#, negative Sr and Eu anomalies and
54 flat rare earth element (REE) patterns of the Idiwhaa gneisses (Fig. 1c) are similar to rocks
55 known as icelandites[22]. Like icelandites, the Idiwhaa gneisses are interpreted by some to record
56 shallow-level fractional crystallization of low-H_2O ('dry') basaltic magmas in which plagioclase
57 was a major fractionating phase[11,16]. However, others propose that icelandites were produced by
58 partial melting of hydrothermally-altered ('wet') basalt[23,24]. As the age of the Idiwhaa gneisses
59 falls near the end of the period of intense meteorite bombardment, and impacts are an efficient
60 means of melting target rocks, either partially or completely[1,2,12,25-30], an origin via impact-
61 induced partial melting of hydrated mafic host rocks seems a plausible petrogenetic model.

62 Here we combine phase equilibria and trace element modelling with hydrodynamic
63 simulations to test the hypothesis that the Idiwhaa gneisses had an origin through impact-induced
64 partial melting. Our phase equilibria modelling uses thermodynamic models appropriate for the
65 partial melting of mafic rocks[31], and allows calculation of the abundance and composition of
66 minerals, melts and fluids as a function of pressure (P), temperature (T) and bulk composition.
67 Trace element modelling uses these data and published mineral/melt partition coefficients[32] to
68 predict the trace element composition of melt as a function of P, T and melt fraction (F). In

69 modelling the petrogenesis of the Idiwhaa gneisses, we take the composition of an average Fe-
70 rich amphibolite host rock from the Acasta gneisses[19] as a putative source (see Methods).
71
72 **Phase equilibria modelling of the Idiwhaa gneisses**
73 A simplified *P–T* phase diagram calculated in the range 0.05–0.80 GPa, 650– 950 ºC is shown in
74 Fig. 2, on which calculated melt fractions (*F*, as mol.%, ~vol.%) are shown as red dotted lines
75 (see Supplementary Fig. 1 for the full phase diagram). The temperature of the onset of partial
76 melting (the H_2O-saturated solidus) decreases from ~730 °C at low pressures (<0.1 GPa) to ~670
77 °C at 0.8 GPa (Fig. 2). Heating beyond the solidus at pressures above 0.3 GPa permits minimal
78 fluid-present melting (< or <<10 mol.%). Thereafter, partial melting proceeds by fluid-absent
79 reactions consuming biotite, hornblende, and quartz until biotite is exhausted at around 730–770
80 °C. Within this *P–T* region (shaded yellow on Fig. 2) melt compositions are granite evolving to
81 granodiorite. Thereafter, fluid absent melting reactions consume hornblende (with or without
82 quartz; green shaded area) to produce melts with lower K_2O/Na_2O ratios typical of TTGs[33].
83 Within the *P–T* window modelled, low pressure TTGs (in which garnet is not stable) are
84 predicted at $P < 0.6$ GPa and medium pressure TTGs, in which garnet but not rutile is stable, at
85 higher *P*.
86 At low pressure *(*$P < 0.27$ GPa) the system remains H_2O-saturated ('wet'; blue region in
87 Fig. 2) to temperatures in excess of 800 °C, and to temperatures in excess of 1,000 °C at 0.1
88 GPa, corresponding to depths of around 3 km. At these low pressures, magnetite is ubiquitous,
89 suprasolidus hornblende is absent and quartz is exhausted almost immediately as the solidus is
90 crossed (Fig. 2; Supplementary Fig. 1). Low pressure melting proceeds by H_2O-saturated

reactions consuming mainly plagioclase and orthopyroxene to produce melts that become successively depleted in SiO_2 and enriched in FeO and MgO as temperature (and *F*) increases.

The calculated major element composition of modelled melts (recalculated on an anhydrous basis) produced at melt fractions of 5–40 mol.% (~vol.%) along isobaric heating paths at 0.1 GPa (blue squares) and 0.5 GPa (pink squares) and along a geothermal gradient of 1,200 °C/GPa (orange squares) are shown in Fig. 1 (see also Fig. 2 and Supplementary Fig. 1), and compared to the compositions of the Idiwhaa gneisses and younger Acasta felsic rocks (assuming $Fe^{3+}/\Sigma Fe = 0.1$). These three paths were chosen as proxies for potential impact-induced melting in the uppermost crust (depth of ~3 km) and mid/lower crust (depth of ~15 km), and for (non-impact) melting along a plausible early Archaean crustal geotherm[33,34], respectively.

Due to the higher thermal stability of quartz with increasing pressure (Fig. 2), melts at 0.5 GPa and along the 1,200 °C/GPa geotherm remain silica rich (SiO_2 > 70 wt%) until melt fractions exceed 25 mol.%, whereas the 0.1 GPa melts fall below this value at melt fractions of 10–15 mol.% (Fig. 1a). In each case the Mg# of the melt increases with increasing *F* (and *T*). Compositionally the modelled melts are unlike Archaean TTGs and the younger Acasta felsic rocks[17], but match well with the Idiwhaa gneisses. In terms of SiO_2 and Mg#, the modelled melts are a good fit with the Idiwhaa gneisses at *F* = 15–35% at 0.1 GPa (produced at ~810–890 °C) and *F* = 30–40 mol.% at 0.5 GPa and along the 1,200 °C/GPa geotherm (~850–900 °C) (Fig. 1a). A similar or slightly more restricted range in *F* (20–35 mol.% at 0.1 GPa; 30–40 mol.% at 0.5 GPa; 35–40 mol.% along the geotherm), requiring *T* > 850 °C, is indicated based on the relative proportions of FeO, MgO and $K_2O + Na_2O$ (Fig. 1b).

Trace element modelling of the Idiwhaa gneisses

Using the calculated abundance of residual minerals formed in equilibrium with melt at different melt fractions (Supplementary Table 2), and mineral/melt partition coefficients appropriate for partial melting of hydrated mafic rocks[32] (Methods and Supplementary Table 3), we model the trace element composition of melts formed at 0.1 GPa, 0.5 GPa and along the 1,200 °C/GPa geotherm (Fig. 3). Relative to the measured composition of the Idiwhaa gneisses (pale blue field in Fig. 3), the modelled trace element compositions of melts produced at 0.5 GPa and along the 1,200 °C/GPa geotherm are depleted in Sr and in all but the lightest rare earth elements (REE), and exhibit no pronounced Eu anomaly (Fig. 3). Other than at $F = 5$ mol.%, melts modelled along the 1,200 °C/GPa geotherm show a pronounced depletion in heavy over middle REE due to the presence of garnet in the residuum (Fig. 3). By contrast, the modelled trace element composition of melts formed at 0.1 GPa at $F \geq 10$ mol.% are an excellent match with the measured composition of the Idiwhaa gneisses.

Our modelled melts produced at 0.1 GPa show a good major element oxide and excellent trace element correspondence with the measured composition of the Idiwhaa gneisses. Thus, the Idiwhaa gneisses could have been the result of 20–35 mol.% (~vol.%) partial melting of hydrated mafic source rocks similar in composition to Fe-rich amphibolites within the AGC, in the uppermost few kilometres of a hydrated mafic crust, requiring temperatures of ~800–900 °C. The occurrence of Fe-rich (now garnet-bearing) amphibolite is restricted to the northeastern part of the AGC, broadly coincident with the Idiwhaa gneisses (fig. 1 in ref. 19). Such Fe-rich mafic rocks are consistent with protracted reworking of thick plateau-like ultramafic to mafic primary crust that is predicted if mantle temperature were significantly warmer than at present[33], and/or the modelled composition of the uppermost 15 km of a fractionated terrestrial magma ocean[35].

137

138 **Hydrocode impact modelling**

139 To test whether our predicted *P* and *T* conditions for formation of the Idiwhaa gneisses are
140 consistent with impact induced melting, we used the Simplified Arbitrary Lagrangian–Eulerian
141 shock physics hydrodynamic code[36] to simulate impact crater formation. For example, the results
142 of models considering a 10 km-diameter dunite projectile with velocities ranging from 12 to 17
143 km s^{-1} impacting a basaltic crust of variable thickness (20–40 km) and variable geothermal
144 gradient (20–40 °C km^{-1}) and underlain by dunitic mantle are shown in Fig. 4 (see Methods and
145 Supplementary Movies 1–8). These models show formation of a ~120-km diameter crater and a
146 hot impact melt pool extending 10–15 km from the impact site. At greater distances, the models
147 predict a layer at temperatures of 800–900 °C and at shallow depths (<3 km) extending up to ~50
148 km radial distance (Fig. 4). This layer is at conditions appropriate to the formation of the Idiwhaa
149 gneisses according to our phase equilibria and trace element modelling.

150 Although no material with conditions appropriate for formation of the Idiwhaa gneisses is
151 predicted in a model considering a projectile of 1 km diameter (that forms a ~15-km diameter
152 crater; Supplementary Fig. 2a; Supplementary Movies 9,10), the model for a 100-km diameter
153 projectile, which forms a crater ~1000-km in diameter, predicts a shallow layer at temperatures
154 between 800 and 900 °C extending between ~200 and 1000 km radial distance from the impact
155 site (Supplementary Fig. 2b; Supplementary Movies 11,12). Recent dynamic modelling of the
156 terrestrial bombardment history suggested that >70% of Earth's surface experienced burial by
157 impact-generated melt since 4.15 Gyrs, with most impacts occurring ~4.15–3.8 billion years
158 ago[1]. Our hydrodynamic modelling shows that, even in the waning stages of bombardment,

layers of shallow partial melting appropriate for the formation of the Idiwhaa gneisses would have been extensive.

Petrogenesis of the Idiwhaa gneisses

The unusual major and trace element composition of the Idiwhaa gneisses has been interpreted to indicate they were formed by shallow (low *P*) fractional crystallization of low-H_2O basaltic magmas, similar to petrogenetic models proposed for modern-day icelandites[16]. However, isotopic and trace element data suggests that an origin for icelandites through partial melting of hydrothermally altered basaltic rocks is also plausible[23,24,37], similar to our petrogenetic model for the Idiwhaa gneisses. Thus, we propose that Earth's oldest known evolved rocks formed through moderate degrees of partial melting of hydrated Fe-rich rocks in the uppermost few kilometres of a fractionated Hadean crust that was dominantly mafic[11,13,38]. Melting at such shallow levels requires temperatures of 800–900 °C or higher and geothermal gradients in excess of ~4,000 ºC/GPa (Fig. 3). Such geotherms are much warmer than those recorded in regional metamorphic rocks of any age worldwide[34], and would require a source of heat beyond what is normally attainable in Earth's crust. We suggest that the required heat was delivered by meteorite impacts towards the end of the post-accretionary bombardment that characterized the first 600 million years of Earth history[1,2]. The flux of meteorites bombarding the Earth during the late Hadean may mean that the predominant mechanism for generating felsic rocks during this time was through impact melting.

References

1 Marchi, S. *et al.* Widespread mixing and burial of Earth's Hadean crust by asteroid impacts. *Nature* **511**, 578–582 (2014).

2 Koeberl, C. Impact processes on the early Earth. *Elements* **2**, 211–216 (2006).

3 O'Neill, C., Marchi, S., Zhang, S. & Bottke, W. Impact-driven subduction on the Hadean Earth. *Nat. Geosci.* **10**, 793–797 (2017).

4 Van Kranendonk, M. J., Bennett, V. & Smithies, H. R. *Earth's oldest rocks*. Vol. 15 (Elsevier, 2007).

5 Wilde, S. A., Valley, J. W., Peck, W. H. & Graham, C. M. Evidence from detrital zircons for the existence of continental crust and oceans on the Earth 4.4 Gyr ago. *Nature* **409**, 175–178 (2001).

6 Mojzsis, S. J., Harrison, T. M. & Pidgeon, R. T. Oxygen-isotope evidence from ancient zircons for liquid water at the Earth's surface 4,300 Myr ago. *Nature* **409**, 178–181 (2001).

7 Valley, J. W., Peck, W. H., King, E. M. & Wilde, S. A. A cool early Earth. *Geology* **30**, 351–354 (2002).

8 Harrison, T. M. *et al.* Geochemistry: Heterogeneous hadean hafnium: Evidence of continental crust at 4.4 to 4.5 Ga. *Science* **310**, 1947–1950 (2005).

9 Harrison, T. M., Schmitt, A. K., McCulloch, M. T. & Lovera, O. M. Early (≥ 4.5 Ga) formation of terrestrial crust: Lu-Hf, $\delta^{18}O$, and Ti thermometry results for Hadean zircons. *Earth. Planet. Sci. Lett.* **268**, 476–486 (2008).

10 Iizuka, T. *et al.* 4.2 Ga zircon xenocryst in an Acasta gneiss from northwestern Canada: Evidence for early continental crust. *Geology* **34**, 245–248 (2006).

11 Reimink, J. R. *et al.* No evidence for Hadean continental crust within Earth's oldest evolved rock unit. *Nat. Geosci.* **9**, 777–780 (2016).

12 Darling, J., Storey, C. & Hawkesworth, C. Impact melt sheet zircons and their implications for the Hadean crust. *Geology* **37**, 927–930 (2009).

13 O'Neil, J. & Carlson, R. W. Building Archean cratons from Hadean mafic crust. *Science* **355**, 1199–1202 (2017).

14 Bowring, S. A. & Williams, I. S. Priscoan (4.00-4.03 Ga) orthogneisses from northwestern Canada. *Contrib. Mineral. Petrol.* **134**, 3–16 (1999).

15 Stern, R. A. & Bleeker, W. Age of the world's oldest rocks refined using Canada's SHRIMP: the Acasta Gneiss Complex, Northwest Territories, Canada. *Geoscience Canada* **25**, 27–31 (1998).

16 Reimink, J. R., Chacko, T., Stern, R. A. & Heaman, L. M. Earth's earliest evolved crust generated in an Iceland-like setting. *Nat. Geosci.* **7**, 529–533 (2014).

17 Reimink, J. R., Chacko, T., Stern, R. A. & Heaman, L. M. The birth of a cratonic nucleus: Lithogeochemical evolution of the 4.02-2.94 Ga Acasta Gneiss Complex. *Precambr. Res.* **281**, 453–472 (2016).

18 Moyen, J. F. The composite Archaean grey gneisses: Petrological significance, and evidence for a non-unique tectonic setting for Archaean crustal growth. *Lithos* **123**, 21–36 (2011).

19 Koshida, K., Ishikawa, A., Iwamori, H. & Komiya, T. Petrology and geochemistry of mafic rocks in the Acasta Gneiss Complex: Implications for the oldest mafic rocks and their origin. *Precambr. Res.* **283**, 190–207 (2016).

20 Iizuka, T., Komiya, T., Rino, S., Maruyama, S. & Hirata, T. Detrital zircon evidence for Hf isotopic evolution of granitoid crust and continental growth. *Geochim. Cosmochim. Acta* **74**, 2450–2472 (2010).

21 Iizuka, T. *et al.* Geology and zircon geochronology of the Acasta Gneiss Complex, northwestern Canada: New constraints on its tectonothermal history. *Precambr. Res.* **153**, 179–208 (2007).

22 Nicholson, H. *et al.* Geochemical and isotopic evidence for crustal assimilation beneath Krafla, Iceland. *J. Petrol.* **32**, 1005–1020 (1991).

23 Bindeman, I. *et al.* Silicic magma petrogenesis in Iceland by remelting of hydrothermally altered crust based on oxygen isotope diversity and disequilibria between zircon and magma with implications for MORB. *Terra Nova* **24**, 227–232 (2012).

24 Martin, E. & Sigmarsson, O. Thirteen million years of silicic magma production in Iceland: links between petrogenesis and tectonic settings. *Lithos* **116**, 129–144 (2010).

25 Gibson, R. Impact-induced melting of Archean granulites in the Vredefort Dome, South Africa. I: anatexis of metapelitic granulites. *J. Metamorph. Geol.* **20**, 57–70 (2002).

26 Grieve, R. A. Petrology and chemistry of the impact melt at Mistastin Lake crater, Labrador. *Geological Society of America Bulletin* **86**, 1617–1629 (1975).

27 Vishnevsky, S. & Montanari, A. Popigai impact structure (Arctic Siberia, Russia): Geology, petrology, geochemistry, and geochronology of glass-bearing impactites. *Special Papers of the Geological Soxciety of America*, 19–60 (1999).

28 Grieve, R. A., Stoeffler, D. & Deutsch, A. The Sudbury structure: Controversial or misunderstood? *Journal of Geophysical Research: Planets* **96**, 22753–22764 (1991).

29 Kring, D. A. & Boynton, W. V. Petrogenesis of an augite-bearing melt rock in the Chicxulub structure and its relationship to K/T impact spherules in Haiti. *Nature* **358**, 141–144 (1992).

30 Pierazzo, E., Vickery, A. & Melosh, H. A reevaluation of impact melt production. *Icarus* **127**, 408–423 (1997).

31 Green, E. C. R. *et al.* Activity-composition relations for the calculation of partial melting equilibria in metabasic rocks. *J. Metamorph. Geol.* **34**, 845–869 (2016).

32 Bédard, J. H. A catalytic delamination-driven model for coupled genesis of Archaean crust and sub-continental lithospheric mantle. *Geochim. Cosmochim. Acta* **70**, 1188–1214 (2006).

33 Johnson, T. E., Brown, M., Gardiner, N. J., Kirkland, C. L. & Smithies, R. H. Earth's first stable continents did not form by subduction. *Nature* **543**, 239–242 (2017).

34 Brown, M. & Johnson, T. Secular change in metamorphism and the onset of global plate tectonics. *Am. Mineral.* **103**, 181–196 (2018).

35 Hofmeister, A. M. Effect of a Hadean terrestrial magma ocean on crust and mantle evolution. *Journal of Geophysical Research* **88**, 4963–4983 (1983).

36 Amsden, A., Ruppel, H. & Hirt, C. *SALE: A simplified ALE computer program for fluid flow at all speeds*. (US Department of Commerce, National Technical Information Service, 1980).

37 Carley, T. L. *et al.* Iceland is not a magmatic analog for the Hadean: Evidence from the zircon record. *Earth. Planet. Sci. Lett.* **405**, 85–97 (2014).

38 Kemp, A. I. S. *et al.* Hadean crustal evolution revisited: New constraints from Pb–Hf isotope systematics of the Jack Hills zircons. *Earth. Planet. Sci. Lett.* **296**, 45–56 (2010).

Corresponding author

All correspondence and requests for materials should be addressed to TEJ (e-mail: tim.johnson@curtin.edu.au).

Acknowledgements

T.E.J. acknowledges financial support from the State Key Lab for Geological Processes and Mineral Resources, China University of Geosciences, Wuhan (Open Fund GPMR210704), and from the Office of Research and Development (ORD) and The Institute of Geoscience Research (TIGeR), Curtin University. KM acknowledges ARC funding and the developers of the iSALE hydrocode. HS publishes with the permission of the Executive Director, Geoscience and Resource Strategy.

Author contributions

TEJ conceived the idea for the paper and did the phase equilibria modelling. TEJ and NJG undertook the trace element modelling. KM performed the hydrodynamic impact modelling. TEJ wrote the manuscript draft. All authors contributed to discussions and the writing of the final paper.

FIGURE CAPTIONS

Fig. 1 | Major element oxide and trace element geochemistry. a, SiO_2 (wt%) vs Mg# [molar Mg/(Mg + Fe^{2+})]. **b**, Ternary diagram with apices FeO, MgO and K_2O + Na_2O (all wt%). The circles show the measured composition [all normalized to 100% in the NCKFMASTO (i.e. anhydrous) compositional system] of rocks: grey dots are Archaean TTGs and potassic rocks[18]; green dots are Acasta felsic gneisses <3.95 Ga in age[17]; red dots are the 4.02 Ga Idiwhaa gneisses[17]. Squares show the composition of modelled melts at 0.1 GPa (blue squares), 0.5 GPa (pink squares) and along a 1,200 °C/GPa geotherm (yellow squares), for which the coloured numbers are melt fractions (*F*) in mol.% (~vol.%). **c**, Primitive mantle normalized trace element compositions of the Idiwhaa gneisses (red) and younger Acasta felsic gneisses (green). The gray field encompasses the average compositions of the different baric types (high, medium and low pressure) of Archaean TTG, including potassic (K) rocks, worldwide[18].

Fig. 2 | Phase equilibria modelling. Simplified *P–T* phase diagram for an average Acasta garnet amphibolite[19] ($n = 6$). The red dotted lines show the proportion of melt (mol.% on a one oxide basis, ~vol.%); the white dashed lines are linear geotherms (°C/GPa) assuming a surface *T* of 25 °C. Within the yellow fields, H_2O-undersaturated melting occurs by reactions consuming biotite and hornblende (± quartz) to produce granitic to granodiorite melts. Within the green fields, H_2O-undersaturated melting occurs by reactions consuming hornblende (± quartz) to produce low pressure TTG melts at $P < 0.6$ GPa and medium pressure TTG melts at higher *P*. The region within the blue fields is characterized by H_2O-saturated ('wet') melting mainly consuming plagioclase and orthopyroxene (and H_2O). The stability of garnet, quartz and magnetite are

indicated. The three large white arrows show the modelled melting paths (isobaric at 0.1 GPa and 0.5 GPa and along a 1,200 °C/GPa geotherm).

Fig. 3 | Trace element modelling. a, Primitive mantle normalized trace element and; **b**, chondrite normalized REE compositions of modelled melts at 0.1 GPa (blue), 0.5 GPa (pink) and along a 1,200 °C/GPa geotherm (yellow) for melt fractions ranging from 5 to 40 mol.%. In each case the pale blue field shows the range of compositions of the Idiwhaa gneisses. For details see Methods.

Fig. 4 | Hydrocode numerical simulation. The modelling considers formation of a Vredefort-like crater made by vertical impact of a 10 km-diameter projectile with a dunite composition travelling at a velocity of 12 km s^{-1} (**a**, **b** and **c**) or 17 kms^{-1} (**d**), impacting basaltic crust with a thickness of 20 km (**a**, **b** and **d**) or 40 km (**c**) that is underlain by dunite mantle. The target temperature gradient (dT/dz) was 20 °C km^{-1} (**a**, **c** and **d**) or 40 °C km^{-1} (**b**). The horizontal lines are simple stratigraphic markers. The blue areas show crust predicted to be at temperatures of 800–900 °C; those at shallow levels (<3 km) are plausible analogues of the Idiwhaa gneisses.

Methods

Phase equilibria modelling. Phase equilibria were modelled in the Na_2O–CaO–K_2O–FeO–MgO–Al_2O_3–SiO_2–H_2O–TiO_2–O (NCKFMASHTO) chemical system using an average Acasta garnet amphibolite[19] (n = 6) assuming an $Fe^{3+}/\Sigma Fe$ ratio of 0.1[39] and an H_2O content of 1.5 wt%. The composition, in terms of the mol.% of the oxides Na_2O–CaO–K_2O–FeO–MgO–Al_2O_3–SiO_2–H_2O–TiO_2–O, is 2.365, 7.386, 0.405, 15.516, 5.520, 9.336, 51.192, 5.341, 2.167, 0.772. Calculations used THERMOCALC version 3.45i[40], the internally consistent thermodynamic data set ds63[41] (updated 5 Jan, 2015) and activity–composition solution models as follows: tonalitic melt, augite and hornblende[31] with a reduced DQF value for the glaucophane end-member of –3 kJ/mol from 0 kJ/mol; garnet, orthopyroxene, biotite and chlorite[42]; olivine and epidote[41]; magnetite–spinel[43]; ilmenite–hematite[44]; $C\bar{1}$ plagioclase and K-feldspar[45] and muscovite–paragonite with a reduced DQF value for the margarite end member of 5 kJ/mol from 6.5 kJ/mol. Quartz, rutile, sphene (titanite), and aqueous fluid (H_2O) are considered as pure end members. Results are shown in an isochemical P–T phase diagram (pseudosection) in the pressure range 0.05 to 0.80 GPa and the temperature range 650 to 950 °C (Supplementary Fig. 1).

The H_2O content in the modelled composition (1.5 wt%) is within the range inferred, based on loss on ignition (LOI) from XRF analyses, for hydrated basaltic rocks sampled from drill core at depths of 2–3 km within hydrothermally altered oceanic crust in Iceland[46]. A quantity of 1.5 wt% H_2O produces minimal H_2O saturated melting (< or << 10 mol.%) at P > 3 kbar (Fig. 2, Supplementary Fig. 1). Assemblage fields are labelled with stable phases, in which abbreviations are as follows: melt (L), garnet (g), augite (aug), orthopyroxene (opx), olivine (ol) hornblende (hb), biotite (bi), magnetite (mt), ilmenite (ilm), plagioclase (pl), K-feldspar (ksp), quartz (q), sphene = titanite (sph), and aqueous fluid (H_2O). All fields contain plagioclase and

ilmenite. The depth of shading of assemblage fields reflects increasing variance. The highest variance fields, opx–hb–L (pl–ilm) and aug–opx–L (pl–ilm), have a variance of 7 (Supplementary Fig. 1). The software and data files used to generate the phase diagrams can be downloaded from: http://www.metamorph.geo.uni-mainz.de/thermocalc.

Trace element modelling. Trace element modelling (Fig. 4) uses the average Acasta garnet amphibolite[19] as a starting composition and the calculated abundance of phases at melt fractions of 5–40 mol.% along the three paths (0.1 GPa, 0.5 GPa and along a 1,200 °C/GPa linear geotherm; see Fig. 2, Supplementary Fig. 2, Supplementary Table 2). Mineral/melt partition coefficients (*D*s; Supplementary Table 3) follow Bédard (2006) that were calculated for anatexis of metabasites[32], with a modified D_{Eu} for plagioclase of 1, based on the range of SiO_2 and MgO contents of the modelled melts[47], and a D_{Ti} for ilmenite of 150[48].

Numerical impact modelling. iSALE-2D (impact Simplified Arbitrary Lagrangian Eulerian)[36,49,50] is a multi-material and multi-rheology finite difference shock physics hydrodynamic code (hydrocode) used for simulating impact processes in 2-D. The code, which can be accessed at: https://isale-code.github.io/>, has been benchmarked against other hydrocodes[51]. A half-space target mesh was divided into two horizontal layers, the crust and the mantle, and a cylindrical symmetry was assumed. The numerical resolution was 20 cells per projectile radius, equating to a numerical cell size of 25 by 25 m for the model involving a 1 km projectile, 250 by 250 m for the model involving a 10 km projectile and 2.5 by 2.5 km for the model involving a 100 km projectile. The impactor speed was taken to be 12 or 17 km s^{-1}, to

accommodate a wide distribution of expected impact speeds during the early terrestrial bombardment[52]—these impact speeds could also represent moderately oblique incidence angles.

The pre-impact crust thickness was fixed to either 20 or 40 km, and the temperature gradient was either 20 or 40 $^{\circ}$C km^{-1}. The material models for the crust (basalt) and mantle and impactor (both dunite) use the appropriate ANEOS-derived equation of state (EOS) tables, as well as the strength[49], failure, and thermal softening models that were used in previous studies for modelling large crater formation on the Moon[53,54] and Mars[55] (Supplementary Table 4). Simulations employ the block-oscillation model of acoustic fluidization to facilitate crater collapse[56]. The role of temperature is restricted to its effect on the shear strength. The material shear strength model in iSALE includes a description of thermal softening: $Y = Y_c \tanh[\varepsilon(T_m/T - 1)]$, where Y_c is the cold shear strength, ε is a material constant, T is temperature, and $T_{\rm m}$ is the melting temperature. We use the Simon approximation to fit the pressure dependence for the melting temperature of anhydrous basalt and KTB peridotite[56] for the crust and mantle, respectively: $T_m = T_{m,0}\,(P/a + 1)^{1/c}$, where $T_{m,0}$ is the melt temperature at zero pressure, P is pressure, and a and c are material constants. The input parameters to our simulations are provided in Supplementary Table 4.

On the Earth, the 10-km projectile is predicted to form a peak-ring crater that is approximately 120 km diameter rim-to-rim. This is comparable to the size of the Vredefort crater[57], the largest confirmed terrestrial impact structure. In Fig. 4 (and Supplementary Fig. 2), horizontal lines show the structural morphology of the crater. Modest structural uplift is present within 20 km radial distance from the impact point. Structural crustal overturn of the top 5–10 km of crustal material is predicted to occur at 20–40 km radial distance. The blue zone denotes material at a temperature of 800–900 $^{\circ}$C. The pre-impact horizontal blue layer at 20 or 40 km

depth is a consequence of the imposed geothermal gradient. However, the blue zone occurring within the crater is a result of impact heating of the target. Specifically, the blue zone within the top 5 km of the crust, which is considered a good proxy for the Idiwhaa gneisses based on phase equilibria and trace element modelling, is a consequence of the process of peak ring formation during the final phase of crater collapse. The diameter of the peak ring is about 60–80 km, in which material at shallow levels and at temperatures of 800–900 °C are predicted to occur along the bulk of its radial distance (Fig. 4a, b and d and, to a lesser extent, c).

Recent numerical modelling of terrestrial bombardment during the Hadean Eon suggested that no substantial large region of the Earth's surface could have survived untouched by impact bombardment[1]. While the early Hadean Eon is suggested to have experienced the largest impact bombardment[1], the later Hadean and early Archean eons should have experienced a significant fraction of the so-called late heavy bombardment.

Data availability. All data supporting the findings of this study are available within the paper, Methods and Supplementary Information.

References only in Methods

39 Berry, A. J., Danyushevsky, L. V., St C. O'Neill, H., Newville, M. & Sutton, S. R. Oxidation state of iron in komatiitic melt inclusions indicates hot Archaean mantle. *Nature* **455**, 960–963 (2008).

40 Powell, R. & Holland, T. J. B. An internally consistent dataset with uncertainties and correlations: 3. Applications to geobarometry, worked examples and a computer program. *J. Metamorph. Geol.* **6**, 173–204 (1988).

41 Holland, T. J. B. & Powell, R. An improved and extended internally consistent thermodynamic dataset for phases of petrological interest, involving a new equation of state for solids. *J. Metamorph. Geol.* **29**, 333–383 (2011).

42 White, R. W., Powell, R., Holland, T. J. B., Johnson, T. E. & Green, E. C. R. New mineral activity-composition relations for thermodynamic calculations in metapelitic systems. *J. Metamorph. Geol.* **32**, 261–286 (2014).

43 White, R. W., Powell, R. & Clarke, G. L. The interpretation of reaction textures in Fe-rich metapelitic granulites of the Musgrave Block, Central Australia: Constraints from mineral equilibria calculations in the system. *J. Metamorph. Geol.* **20**, 41–55 (2002).

44 White, R., Powell, R., Holland, T. & Worley, B. The effect of TiO_2 and Fe_2O_3 on metapelitic assemblages at greenschist and amphibolite facies conditions: mineral equilibria calculations in the system K_2O–FeO–MgO–Al_2O_3–SiO_2–H_2O–TiO_2–Fe_2O_3. *J. Metamorph. Geol.* **18**, 497–512 (2000).

45 Holland, T. & Powell, R. Activity-compositions relations for phases in petrological calculations: An asymetric multicomponent formulation. *Contrib. Mineral. Petrol.* **145**, 492–501 (2003).

46 Marks, N., Zierenberg, R. A. & Schiffman, P. Strontium and oxygen isotopic profiles through 3km of hydrothermally altered oceanic crust in the Reykjanes Geothermal System, Iceland. *Chem. Geol.* **412**, 34–47 (2015).

47 Bédard, J. H. Trace element partitioning in plagioclase feldspar. *Geochim. Cosmochim. Acta* **70**, 3717–3742 (2006).

48 Xiong, X. *et al.* Experimental constraints on rutile saturation during partial melting of metabasalt at the amphibolite to eclogite transition, with applications to TTG genesis. *Am. Mineral.* **94**, 1175–1186 (2009).

49 Collins, G. S., Melosh, H. J. & Ivanov, B. A. Modeling damage and deformation in impact simulations. *Meteoritics & Planetary Science* **39**, 217–231 (2004).

50 Wünnemann, K., Collins, G. & Melosh, H. A strain-based porosity model for use in hydrocode simulations of impacts and implications for transient crater growth in porous targets. *Icarus* **180**, 514–527 (2006).

51 Pierazzo, E. *et al.* Validation of numerical codes for impact and explosion cratering: Impacts on strengthless and metal targets. *Meteoritics & Planetary Science* **43**, 1917–1938 (2008).

52 Bottke, W. F. *et al.* An Archaean heavy bombardment from a destabilized extension of the asteroid belt. *Nature* **485**, 78–81 (2012).

53 Ivanov, B., Melosh, H. & Pierazzo, E. Basin-forming impacts: Reconnaissance modeling. *Geological Society of America Special Papers* **465**, 29–49 (2010).

54 Miljković, K. *et al.* Subsurface morphology and scaling of lunar impact basins. *Journal of Geophysical Research: Planets* **121**, 1695–1712 (2016).

55 Pierazzo, E., Artemieva, N. & Ivanov, B. Starting conditions for hydrothermal systems underneath Martian craters: Hydrocode modeling. *Geological Society of America Special Papers* **384**, 443–457 (2005).

56 Melosh, H. & Ivanov, B. Impact crater collapse. *Annual Review of Earth and Planetary Sciences* **27**, 385–415 (1999).

57 Turtle, E. P., Pierazzo, E. & O'Brien, D. P. Numerical modeling of impact heating and cooling of the Vredefort impact structure. *Meteoritics & Planetary Science* **38**, 293–303 (2003).

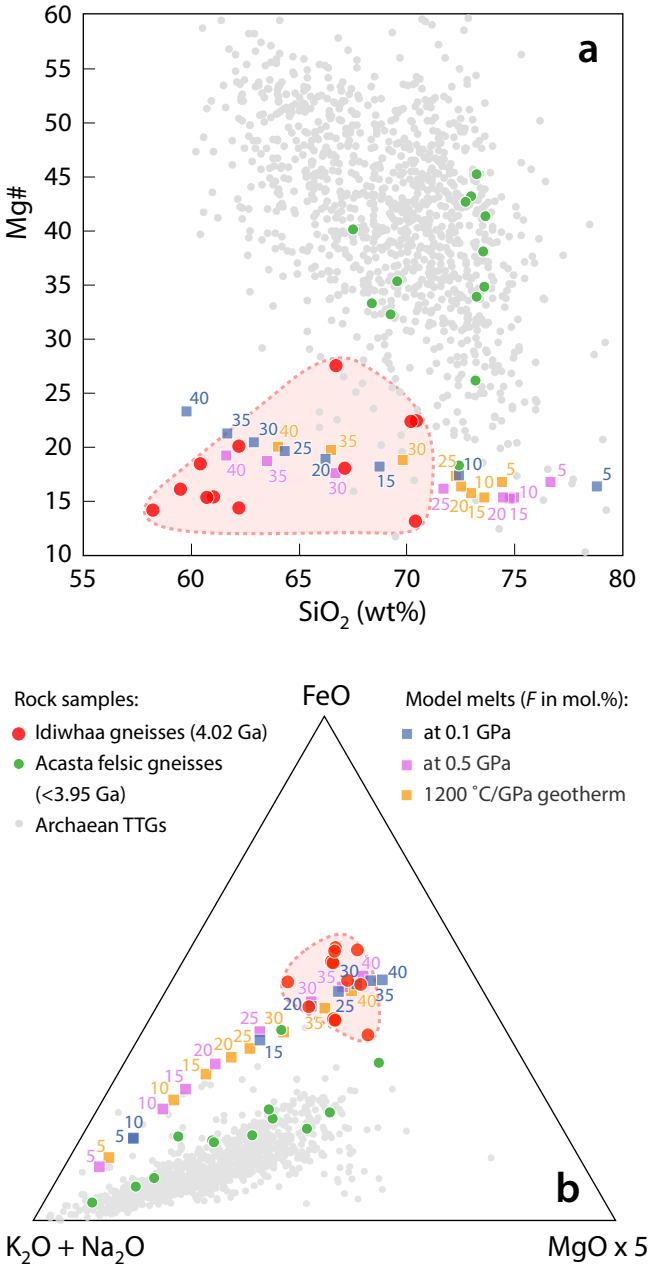

Johnson et al. Fig. 1

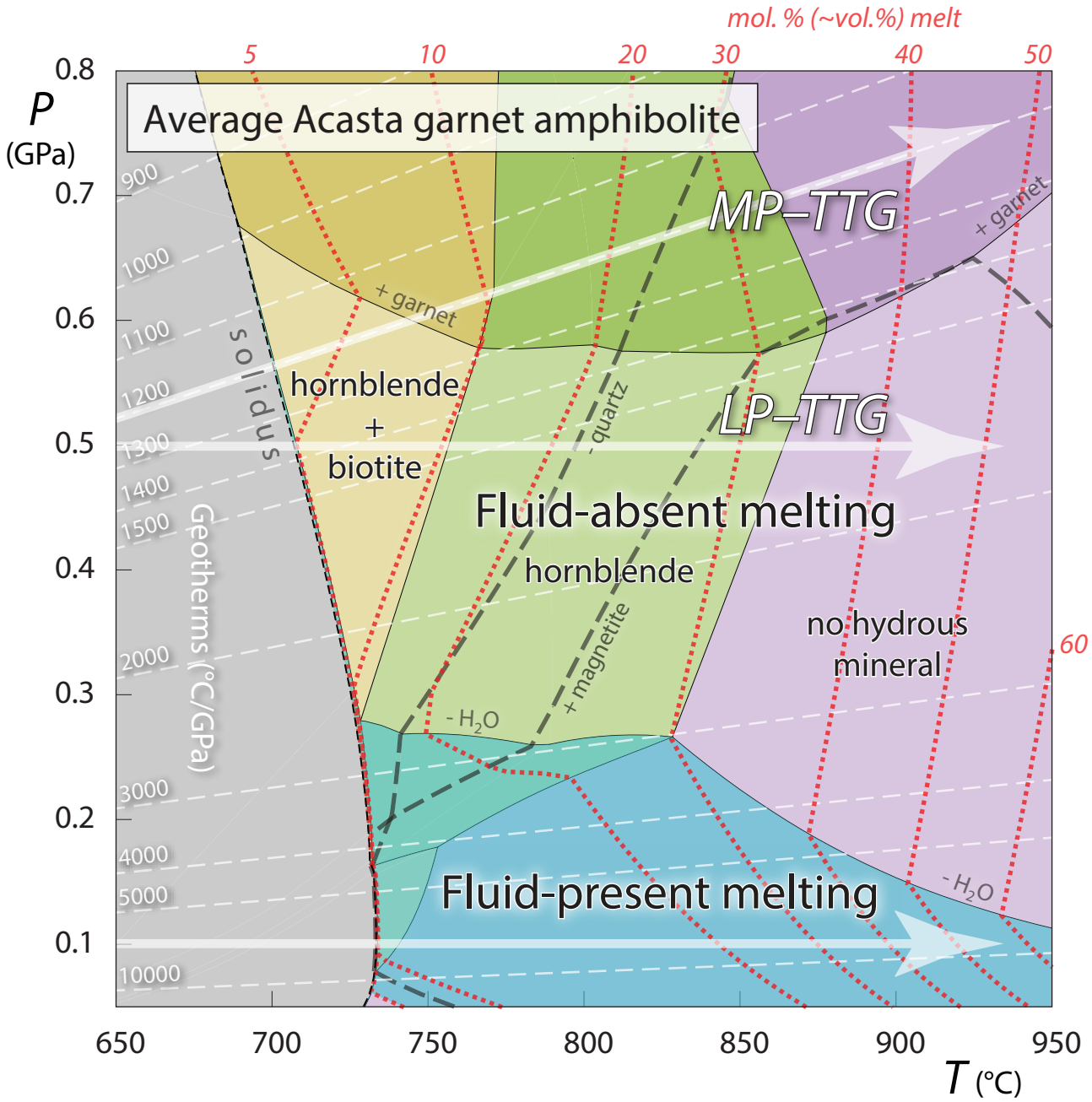

Johnson et al. Fig. 2

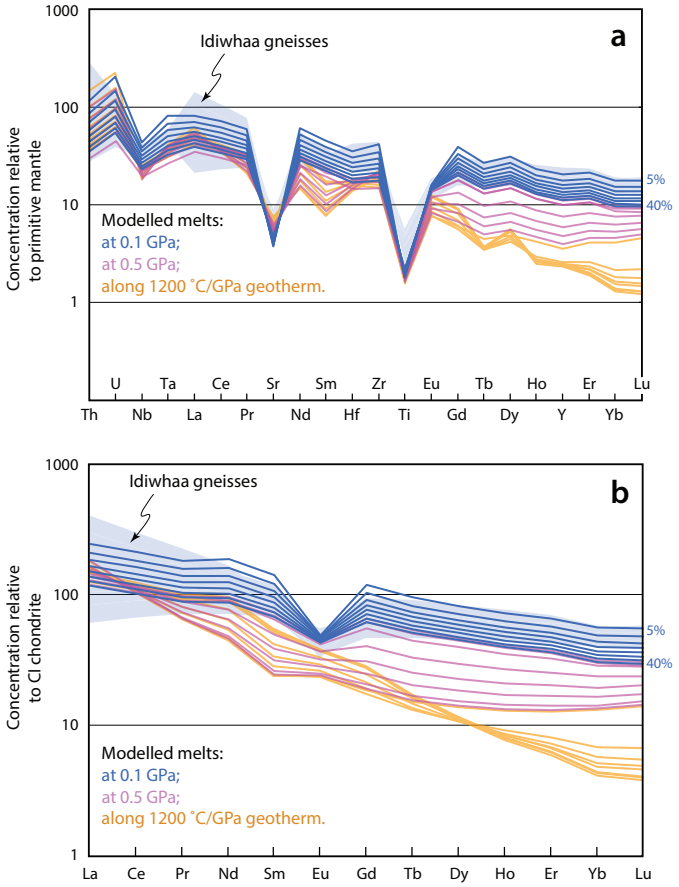

Johnson et al. Fig. 3

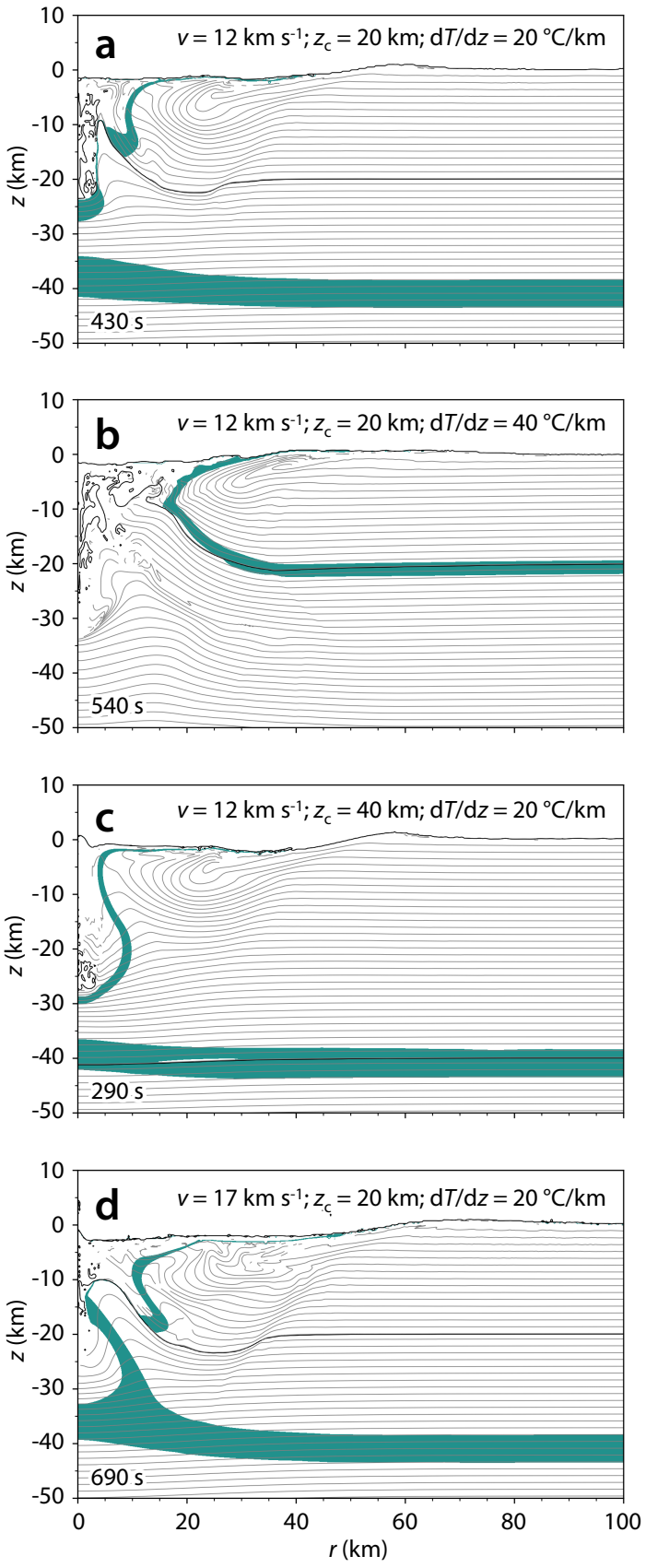

Johnson et al. Fig. 4